High-Resolution *GOES-8* Visible and Infrared Cloud Frequency Composites over Northern Florida during the Summers 1996–99

BERNADETTE H. CONNELL

Cooperative Institute for Research in the Atmosphere, Colorado State University, Fort Collins, Colorado

KENNETH J. GOULD

National Weather Service, Tallahassee, Florida

JAMES F. W. PURDOM

Office of Research and Applications, NOAA/National Environmental Satellite, Data, and Information Service, Camp Springs, Maryland

(Manuscript received 22 January 2001, in final form 6 July 2001)

ABSTRACT

GOES-8 visible and infrared cloud frequency composites have been created from imagery collected during June, July, and August for the years 1996–99 over northern Florida. These cloud frequency composites are unique because they offer high-resolution coverage over a small area and have been tailored to address forecast needs. Both monthly and regime cloud frequency composites are presented. Nine regimes were designated to reflect the strength and development of the sea-breeze front under various synoptic winds and the resulting effect on convective development. The regimes were designated by mean boundary layer wind speed and direction over the region of interest. Results from four of the regimes are presented.

A total of 222 days (60% of all possible days) were designated for the various wind regimes. Regime 4 (W to SW flow) occurred most frequently (24%) and had the most widespread distribution of higher cloud frequency, occurring both near the coast and inland. Regime 2, with contrasting E to NE flow, was the next most frequently occurring regime (17%) and had lower cloud frequencies, particularly inland in Alabama and Georgia. Regime 5, with strong W to SW flow (15%, not presented) was third, followed by Regime 8 with N to NW flow (13%) and Regime 1 (11%) with light and variable or light SE flow.

The monthly composites included the days from the various regime days as well as those with a completely disturbed or completely suppressed sea-breeze circulation. Nonetheless, the influence of the sea-breeze circulation can readily be seen in the diurnal progression of cloud frequency over a month. The variations seen in monthly cloud frequency composites for June, July, and August 1996–99 highlight periods of high and low cloud frequency and offer a different perspective on year-to-year and month-to-month variability.

The regime cloud frequency results are actively being used during the summer season in aviation and public forecasting to supplement available information.

1. Introduction

Many satellite-based cloud frequency studies have focused on obtaining knowledge of the characteristics and distribution of clouds and how they affect the earth's climate. A primary user of this information has been the global climate modeling community. Many of the datasets have been collected at a coarse resolution (e.g., Schiffer and Rossow 1983) and offer limited information to a forecaster wanting to use the information for a local region. A few studies have looked at cloud frequency derived from visible imagery over local areas. For example, the work of Klitch et al. (1985) and Gibson and Vonder Haar (1990) has contributed to our understanding of initiation and feedback mechanisms on the mesoscale and the influence and interaction with the synoptic scale.

Much of the convection over the Florida panhandle and peninsula during June, July, and August is directly related to the sea-breeze circulation. Blanchard and López (1984) summarized observational and numerical model results conducted over south Florida since 1948. These studies indicate that there is a strong relationship between convection, the sea breeze, and large-scale synoptic flow, as well as small-scale surface characteristics that reveal a complex interaction of scales. These complex interactions make forecasting the timing, location, and intensity of convection a challenging task.

Corresponding author address: Dr. Bernadette H. Connell, Cooperative Institute for Research in the Atmosphere, Colorado State University, Foothills Campus Fort Collins, CO 80523-1375.
E-mail: connell@cira.colostate.edu

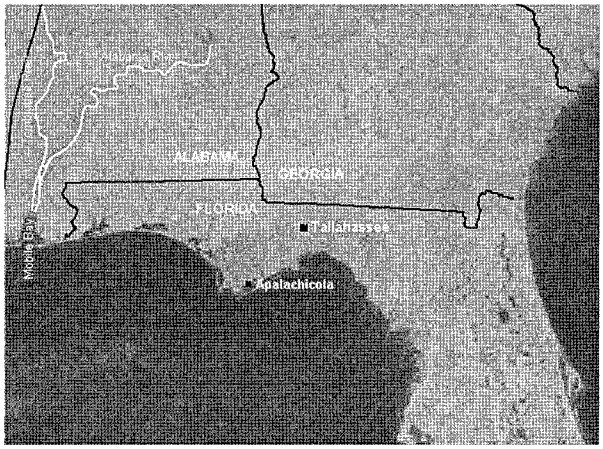

FIG. 1. *GOES-8* visible cloud-free background composite for 1615 UTC Jul 1999. This image shows the area of coverage for the study as well as locations for Tallahassee, Apalachicola, and various rivers described in the text.

The primary differences between the cloud frequency study presented here and other cloud climatology composites are the small area of focus, stratification into regimes, and the high resolution of the satellite imagery. The results presented here are a continuation of the work started by Gould and Fuelberg (1996) for northern Florida. In their initial study, the analysis looked at average digital brightness values of visible imagery and provided a qualitative view of cloud frequency under different synoptic regimes. The analysis has shifted from qualitative to quantitative by compositing cloud/no-cloud information from visible imagery as well as compositing cloud frequency by temperature threshold of the *Geostationary Operational Environmental Satellite-8* (*GOES-8*) infrared (10.7 μm) imagery.

Results are presented from regimes of cloud frequency composites derived from *GOES-8* hourly visible and infrared imagery collected during June, July, and August, over a 4-yr period (1996–99). We present regime composites as well as the monthly composites to highlight a number of features. The first is the unique information obtained from using high-resolution imagery. The second is the information obtained when the imagery are stratified into regimes. We also discuss the characteristics of each regime and potential significance in forecasting convection.

2. Data and methodology

a. GOES-8 *visible and 10.7-μm data collection and preparation*

Hourly *GOES-8* full-resolution visible (1 km) and 10.7-μm imagery (4 km) centered over Tallahassee, Florida (TLH), for June, July, and August of 1996–99 were used in this study (see Fig. 1 for the study area). The imagery were collected and archived at the Cooperative Institute for Research in the Atmosphere (CIRA). Visible imagery were archived hourly between 1315 and 2215 UTC, while the 10.7-μm imagery were archived hourly between 0015 and 2315 UTC. Image processing and analysis were done on personal computers with the Man computer Interactive Data and Analysis System (McIDAS) software (Lazzara et al. 1999). McIDAS is the software backbone for the Regional and Mesoscale Meteorology Advanced Meteorological Satellite Demonstration and Interpretation System (Molenar et al. 2000), which has been demonstrated at several National Weather Service (NWS) offices.

Both the visible and 10.7-μm imagery were archived at the highest resolution available to cover the same spatial area surrounding Tallahassee. The *GOES-8* satellite oversamples the instantaneous geometric field of view for the 1-km visible and 4-km infrared imagery by a factor of 1.75 in the east–west direction (Menzel and Purdom 1994). The 1-km visible imagery viewed at the NWS office is centered over Tallahassee and displays every line and every other element on a 480 line $\times$ 640 element monitor, and it is that imagery that were used for this study. The *GOES-8* 10.7-μm imagery is available at 4-km resolution and every line and element were collected for a 120 $\times$ 320 image to correspond to the same display area as the visible imagery.

Since threshold techniques (to be described below) were used to analyze the data, each image was converted from 10-bit GOES variable format (GVAR) to 1-byte (brightness counts) to reduce the volume of data being archived. This made the dataset manageable and amenable to being placed on CD-ROM for easy access through a variety of display and analysis programs.

The visible cloud frequency composites were created by the threshold technique in which a background cloud-free image is compared with a normal visible scene to discriminate between cloudy and cloud-free areas. This technique has been used in numerous regional and mesoscale studies, for example, Gibson and Vonder Haar (1990), Reinke et al. (1992), and Klitch et al. (1985).

A brief description of the visible threshold technique follows. Before the imagery were composited into the designated regimes, they were analyzed hour by hour for each month to obtain representative backgrounds. The choice of the representative background image for each hour of each month is challenging for a number of reasons: 1) the visible albedo representing the surface will vary throughout the day due to the change of the sun angle, 2) the albedo will also vary due to changes in vegetative characteristics over time and even to changes in surface moisture, 3) a high frequency of clouds at a particular time makes it difficult to obtain cloud-free regions, and 4) the *GOES-8* visible albedo measurements have degraded over the years of operation (Knapp and Vonder Haar 2000). To help alleviate the problems associated with reasons 1 and 3, an albedo correction based on the solar angle was applied to the visible imagery (Kidder and Vonder Haar 1995).

After the imagery were corrected for the albedo variation due to the change of the sun angle, all imagery were navigated to a single reference image using geographic reference points that had strong contrast such as coastline features, lakes, and rivers. After three years of data collection, warping of the imagery occurred such that geographic features on the western edge of the region were shifted a pixel to the left. Concurrently, geographic features on the eastern edge of the region were shifted a pixel to the right. Wherever possible, images were navigated to the center of the region to minimize error.

The next step of the process created the background or cloud-free image from the navigated imagery for each hour of each month to check for the lowest brightness count (darkest value) for each pixel over the images for the month. An example of a cloud-free image for 1615 UTC July 1999 is shown in Fig. 1. The cloud-free image was then used to discriminate cloud versus no-cloud regions in each image for the specified times. The series of images for a particular hour over the month are then compared pixel by pixel with the background image. If the pixel in the image is brighter by 20 brightness counts than the pixel in the background image, it is designated as cloud. This method does not distinguish between low- or high-level clouds, nor does it distinguish type of cloud such as convective or stratiform.

Visual inspection of the data showed that there were instances when the 20 brightness count threshold was not ideal for the discrimination of clouds from the background. For example, during June of 1998, smoke from fires in Central America was detected as cloud, particularly for times close to sunrise and sunset. The analysis here did not focus on imagery near sunrise and sunset. For select instances where smoke posed a noticeable problem at other times, the threshold was increased to 25–30 brightness counts.

The threshold technique for the 10.7-μm imagery is a much simpler process that utilizes the brightness temperature to distinguish between cloudy and cloud-free regions. One of the objectives of using the 10.7-μm imagery was to see how closely the visible and 10.7-μm cloud frequency composites matched. Another objective was to analyze cloud cover at night, and a third objective was to distinguish deep convection. June, July, and August are warm months in Florida, with 68.4°F (293.2 K) being the coldest temperature recorded for a 30-yr period (1961–90) (Available from Southeast Regional Climate Center at http://www.dnr.state.sc.us/climate/sercc). With this in mind, the threshold temperature of 283 K was chosen to distinguish between cloudy and clear ''background'' regions. Pixels equal to or colder than this value were designated as cloudy.

A threshold of 235 K was used to determine the frequency and location of deep convection. This threshold temperature has been used in other studies, (e.g., Garreaud and Wallace 1997), and corresponds to cloud-top height above the 300-hPa level. This threshold technique, however, does not distinguish between cirrus and convective cloud.

TABLE 1. NWS Tallahassee summer sea-breeze regimes.

Regime	Description
1	Light and variable or light SE (<3 kt)
2	Light to moderate (3–10 kt) E to NE
3	Strong (>10 kt) E to NE
4	Light to moderate (3–10 kt) W to SW
5	Strong (>10 kt) W to SW
6	Moderate (6–10 kt) SE to S
7	Strong (>10 kt) SE to S
8	Light to moderate (3–10 kt) N to NW
9	Strong (>10 kt) N to NW

b. Synoptic regime designation

Each day was designated with a particular synoptic flow regime based on the low-level boundary layer wind. Blanchard and López (1985) and Gould and Fuelberg (1996) and many other Florida researchers and operational meteorologists have found that the 1200 UTC 1000–700-hPa mean layer vector wind (MLVW) to be most representative of the synoptic steering flow for its influence on the sea-breeze circulation. The MLVW was calculated using PC-Grid Interactive Display and Diagnostic System software for 1996–98, and the Advanced Weather Information Processing System during 1999, using both the Eta Model and Nested Grid Model output. The designated regimes are shown in Table 1.

Light to moderate wind speeds are separated from stronger wind speeds because of the different effects on the development and inland penetration of the sea breeze. Opposing synoptic flow, as is found in regimes 8 and 9, inhibits the inland penetration of the sea breeze, but can also enhance convergence and upward vertical motion along the sea-breeze front. Conversely, onshore synoptic flow aids the inland penetration of the sea breeze, but limits the development of convergence along the sea breeze. The regimes do not fall into strict numerical bins on the compass, but rather allow for user input on the synoptic interpretation of both the current situation and the evolution of the flow patterns.

The results of four regimes representing opposing synoptic flows are presented (regimes 1, 2, 4, and 8). The following descriptions reflect the dominant synoptic flow patterns and the relative frequency of occurrence of the various regimes determined from studies conducted over south Florida. They also reflect what operational meteorologists at TLH believed to be representative of the region when the study was initiated. Schematics of the synoptic wind patterns at 1000 and 700 hPa can be found in Blanchard and López (1984, 1985).

Under regime 1, the Bermuda high, the semipermanent subtropical high of the North Atlantic Ocean, is the dominant synoptic feature. Because of the westward

TABLE 2. Number of days designated for various wind regimes during the period Jun, Jul, and Aug of 1996–99.

Regime	1	2	3	4	5	6	7	8	9	Total
No. of days	25	38	13	54	33	12	5	30	12	222
No. of days missing	0	1	0	1	2	0	1	3	1	9

termination of the ridge axis, the Florida panhandle is left in a cull point and experiences light and variable winds or light southeast winds. This regime is typical for a normal summer and occurs frequently. This pattern follows type 1 of Blanchard and López (1984, 1985).

Another common regime during the summer is regime 4, resulting when the Bermuda high is shifted farther to the south. This synoptic pattern sets up a general west-southwest flow (3–10 kt) over the Florida panhandle, generating favorable thermodynamics for more widespread convective development. This regime follows type 3 of Blanchard and López (1984, 1985).

Regime 2 is characterized by a high pressure system of continental origin located to the north and east of the area. This produces a general easterly flow (3–10 kt) over the region, and with less favorable thermodynamics, convection is more limited on this type of day. This regime is less common during a typical summer and follows type 2 of Blanchard and López (1984, 1985).

Regime 8 also occurs less often during a typical summer. This regime usually occurs after passage of a cold front or trough and the winds shift to the north-northwest (3–10 kt). Although the flow is offshore, keeping the sea breeze near the coast (along the panhandle) later in the day, the opposing flow also allows for a more intense sea-breeze front. If the thermodynamics are favorable, there is potential for severe weather later in the day.

c. Image compositing for the regimes

After the days were designated for the various flow regimes and the images were checked for navigation and distinguished as cloud/no cloud, they were ready for compositing. The compositing for the visible imagery was done on an hour-by-hour basis from 1415 to 2115 UTC. Low sun angles prevented the use of imagery before 1415 UTC at the beginning of the day and after 2115 UTC at the end of the day, particularly for July and August.

Imagery for the 10.7-μm channel were available for a 24-h period, which dictated a different compositing time period from that of the visible imagery. Since the end of the convective day did not correspond to 2315 UTC, the 10.7-μm imagery for a particular regime day were analyzed from 0715 UTC of the current day to 0615 UTC of the next day [2315–2215 eastern daylight time (EDT)]. Images were composited for June, July, and August from 1996–99.

For each image of the designated regime and hour, the number of pixels containing clouds was summed on a pixel-by-pixel basis. The sum was then divided by the total number of days possible for that particular regime and hour. The result was multiplied by 100 to obtain the cloud frequency. The output was then placed back into a digital image and stretched between 50 and 250 brightness counts.

3. Results

Information on the number of days designated for the various regimes by the Tallahassee Weather Forecast Office is presented in Table 2. Also shown is the number of entire days for which satellite data are missing. Those days not designated for particular regimes were either completely disturbed synoptically; affected by a tropical system, cold front, or mesoscale convective system; or the sea breeze was completely suppressed. The number of days designated composed 60% of all possible days.

A recent paper by Camp et al. (1998) used cloud-to-ground lighting data to examine the distribution of lightning across the Florida panhandle in relation to the low-level synoptic flow for the period 1 May–31 October for 1989–94. Their regimes closely reflect the regimes used in this study. The times of the maximum number of lightning flashes were found to be variable over their regimes but overall occurred between 1800 and 2200 UTC. The first results presented here are the cloud frequencies for 1715 UTC and focus on a small area within the region of analysis. This time is chosen to capture the distribution of small-scale cumulus clouds before the period of maximum deep convection is reached and the area is chosen to highlight small-scale features noted in Gibson and Vonder Haar (1990) and Rabin and Martin (1996).

a. Morning regime composites

Cloud frequency composites for 1715 UTC for regimes 1, 2, 4, and 8 are presented in Fig. 2. The number of days used to create each of the composites is shown on the image (n = sample size). This number may differ from the total number of days designated in Table 2 due to bad or missing satellite images for a particular hour. Some interesting features show up in the composites in Fig. 2 that highlight similarities and differences of the wind stratification.

Attention is drawn to ''opposing'' regime pairs: regimes 1 and 8 and regimes 2 and 4. At the coast to the N-NE of Apalachicola along line X, regime 1 (light and variable flow; Fig. 2a) shows higher cloud frequencies perpendicular and just inland from the coast, indicating

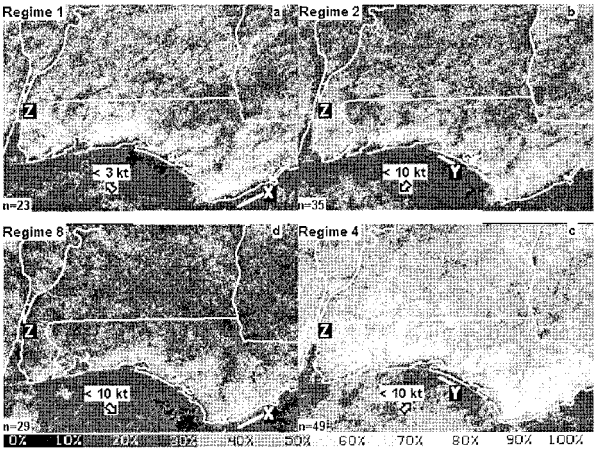

FIG. 2. *GOES-8* visible cloud frequency composites for 1715 UTC for (a) regime 1, (b) regime 2, (c) regime 4, and (d) regime 8. The number of images used to create each composite is shown in the lower-left corner of each image (n = sample size). The study period includes Jun–Aug for 1996–99. The arrows and wind speeds correspond to the background synoptic conditions for each regime as summarized in Table 1.

how far the sea-breeze front has advanced inland at this time under variable or light southerly to southeasterly flow. Measurements on the imagery estimate this distance at 10 km. In contrast to this, regime 8 (N to NW flow; Fig. 2d) show cloud cover located at the coast along line X, indicating that the sea-breeze front has been held along the coast by the northerly flow.

At the coast to the N–NW of Apalachicola along line Y, regime 2 (E to NE flow; Fig. 2b) displays cloud cover located at the coast, indicating that the northeasterly flow has not allowed the inland progression of the sea-breeze front. In contrast, for regime 4 (W to SW flow; Fig. 2c), cloud cover along the same stretch of coast corresponding to line Y is seen farther inland indicating that the sea-breeze front has advanced farther inland at this time in response to the background westerly to southwesterly flow. Measurements on the imagery estimate this distance at 6 km.

Gibson and Vonder Haar (1990) pointed out cloud-free regions in their image composites early in the day. These cloud-free regions coincide with rivers and bays and associated areas downwind and reflect the divergent flows over the water bodies due to differential heating between the land and water. These features show up in the various regimes in Fig. 2. Clearer regions are noted in all regimes north of Mobile Bay (point Z in Fig. 2, along the Alabama and Tombigbee Rivers shown by the white line and identified in Fig. 1). The less cloudy regions are shifted slightly to the west when the flow is from the E to NE (regime 2; Fig. 2b), and the less cloudy regions are shifted slightly to the east when the flow is from the W to SW (regime 4; Fig. 2c).

These two examples of the position of the sea breeze

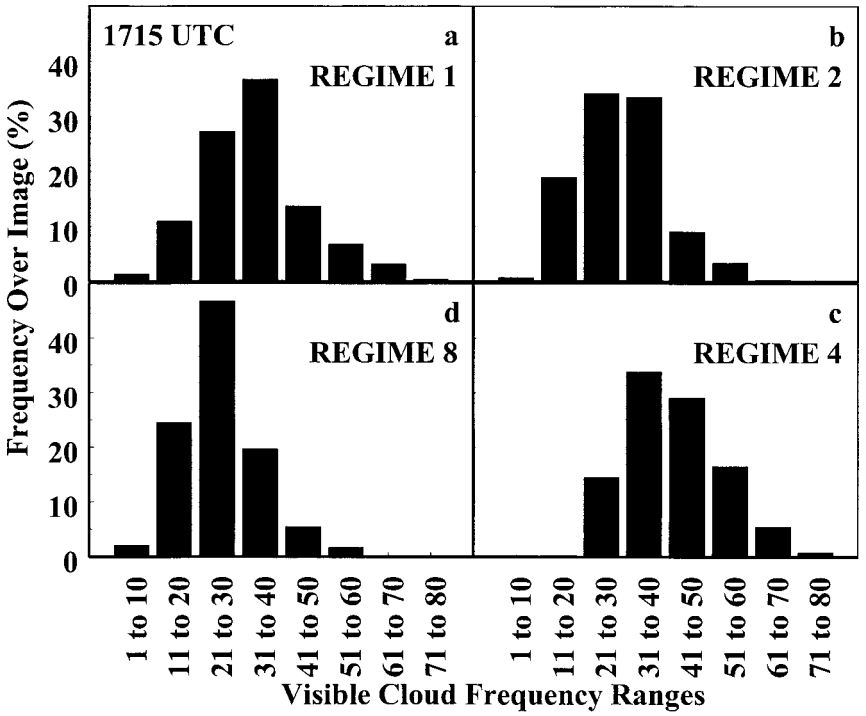

FIG. 3. Histograms of the frequency of cloud occurrence for 1715 UTC for the visible composites shown in Fig. 2 for (a) regime 1, (b) regime 2, (c) regime 4, and (d) regime 8. The x axis represents bins of 10% cloud frequency and the y axis shows the corresponding percentage of occurrence.

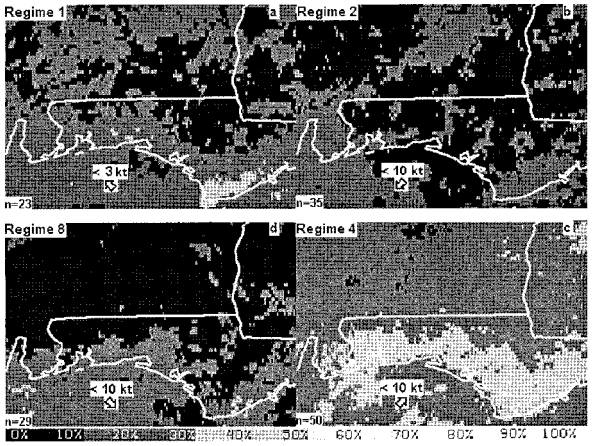

FIG. 4. *GOES-8* 10.7-μm cloud frequency composites by temperature threshold (283 K) for 1715 UTC for (a) regime 1, (b) regime 2, (c) regime 4, and (d) regime 8. The study period includes Jun–Aug for 1996–99. The arrows and wind speeds correspond to the background synoptic conditions for each regime as summarized in Table 1 (n = sample size).

relative to the regimes and the position of the clouds around rivers in relation to the regimes demonstrate some of the small-scale variability and differences that can be detected from the high-resolution visible image composites.

Histograms (Fig. 3) were created for each of the images presented in Fig. 2 to help quantify the difference in cloud frequency noted between the regimes. The x axis represents bins of 10% cloud frequency and the y axis shows the corresponding percentage of occurrence for the respective images. There is only a small area between all the regimes that show cloud frequencies greater than 60% for this time of day; regimes 2 and 8 have less than 1% area greater than 60% and regimes 1 and 4 have 3% and 5%, respectively, greater than 60% cloud frequency. Regime 4 (W to SW flow) has the largest number of days for the composite and has the most widespread distribution and higher frequencies of clouds for the area shown. Regimes 1, 2, and 8 have 76%, 87%, and 92%, respectively, of their pixels with cloud frequencies less than 40%, while regime 4 has 48% of the pixels with cloud frequencies less than 40%.

The last two figures for this morning composite section reveal what the 10.7-μm threshold technique detected for cloud frequency and how this compares with what was detected for the visible cloud frequency composites at the same time. Figure 4 shows the cloud frequency results based on the 283-K threshold for 10.7-μm imagery for regimes 1, 2, 4, and 8 at 1715 UTC to correspond with the visible cloud frequency composites presented in Fig. 2. The 10.7-μm composites at this time generally show the same cloud frequency pattern as the visible composites, but with significantly less cloud frequency. Poor correlation is found between the

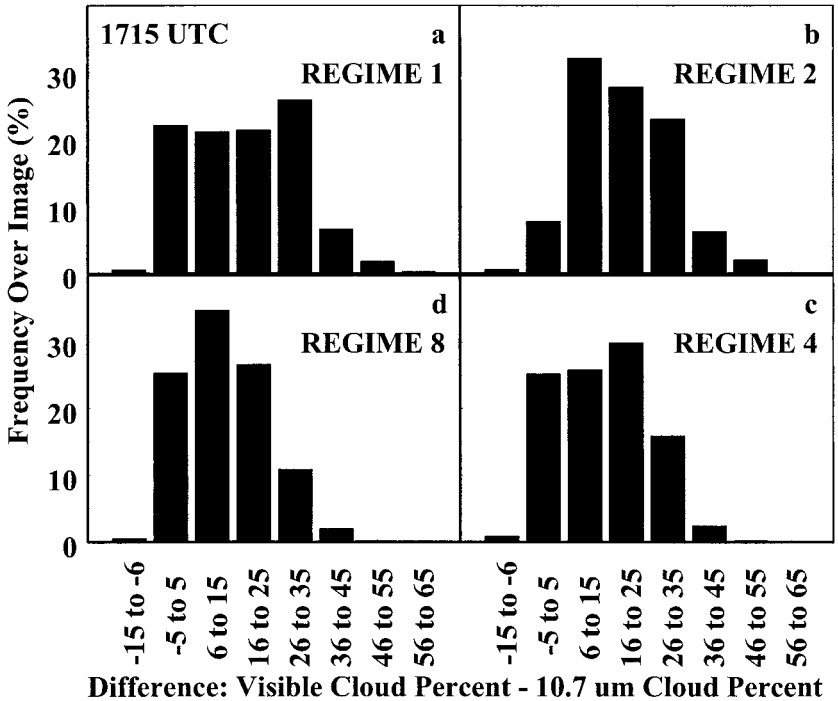

FIG. 5. Histograms of the difference of cloud frequency between the visible composites (Fig. 2) and the 10.7-μm composites (Fig. 4) for 1715 UTC for (a) regime 1, (b) regime 2, (c) regime 4, and (d) regime 8. The x axis represents bins of 10% cloud frequency and the y axis shows the corresponding percentage of occurrence. The -5 to 5 range represents no difference.

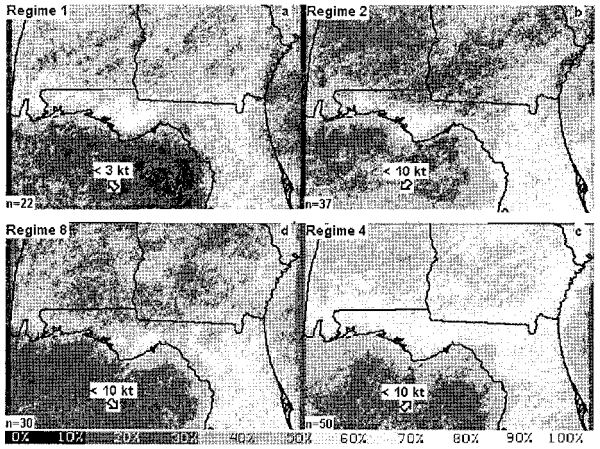

FIG. 6. *GOES-8* visible cloud frequency composites for 2115 UTC for (a) regime 1, (b) regime 2, (c) regime 4, and (d) regime 8. The number of images used to create each composite is shown in the lower-left corner of each image (n = sample size). The study period includes Jun–Aug for 1996–99. The arrows and wind speeds correspond to the background synoptic conditions for each regime as summarized in Table 1.

visible and 10.7-μm areas, with correlation coefficient $r = 0.13$, 0.14, 0.28, and 0.23, respectively, for regimes 1, 2, 4, and 8. Some of the general features found in the composites are reiterated here: (a) higher cloud frequencies occur near coastal areas, and (b) regime 4 has the most cloud coverage for area and frequency, with regime 1 showing the next greatest coverage. The 10.7-μm composites also do not reveal as much detail in the cloud pattern as the visible composites.

The difference between the 10.7-μm and the visible image composites is mainly due to differences in resolution. At 1715 UTC, the predominant clouds are small cumulus. The *GOES-8* visible imagery is being sampled at 1-km resolution and will therefore capture clouds that are 1 km or larger in scale. The 10.7-μm imagery is being sampled at 4-km resolution. A cloud on the order of 1 km will ''occupy'' 1/16th of the field of view. The other 15/16ths of the field of view will see the warmer background surface. Overall, the satellite senses a warmer temperature and a cloud will not be detected by the temperature threshold technique. This results in lower cloud frequency as well as less detail for the 10.7-μm imagery compared to the visible imagery.

Histograms of cloud frequency differences—visible cloud frequency $-$10.7-μm cloud frequency for each of the regimes—are shown in Fig. 5. In order to do the differencing, the 10.7-μm pixels were duplicated to match the resolution of the visible imagery. The x axis in Fig. 5 shows the bins associated with the amount of difference between the two techniques, and the y axis shows the frequency of occurrence over the image. We consider $\pm$5% frequency difference to represent no difference between the composites. The ''no difference''

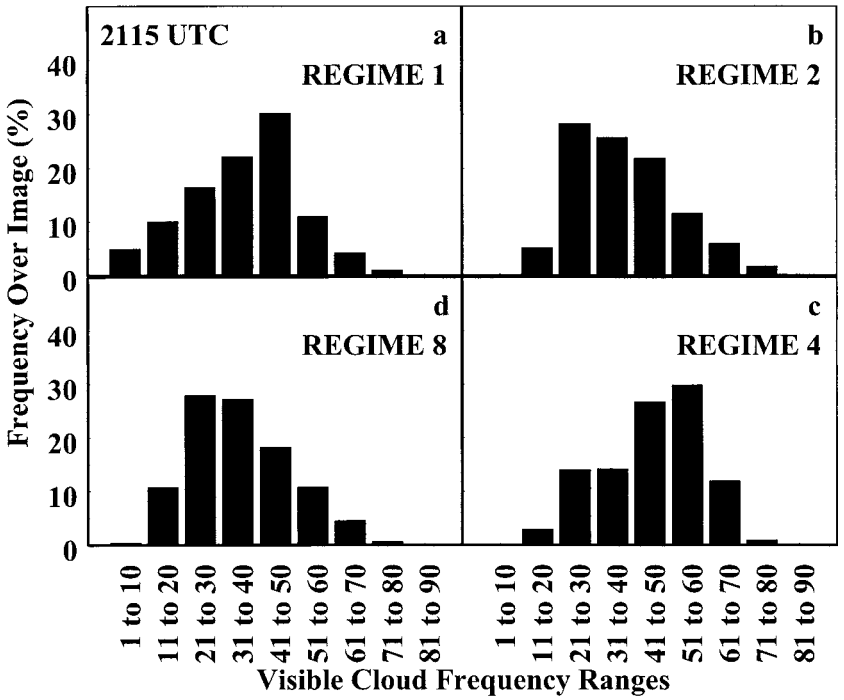

FIG. 7. Histograms of the frequency of cloud occurrence for 2115 UTC for the visible composites shown in Fig. 6 for (a) regime 1, (b) regime 2, (c) regime 4, and (d) regime 8. The x axis represents bins of 10% cloud frequency and the y axis shows the corresponding percentage of occurrence.

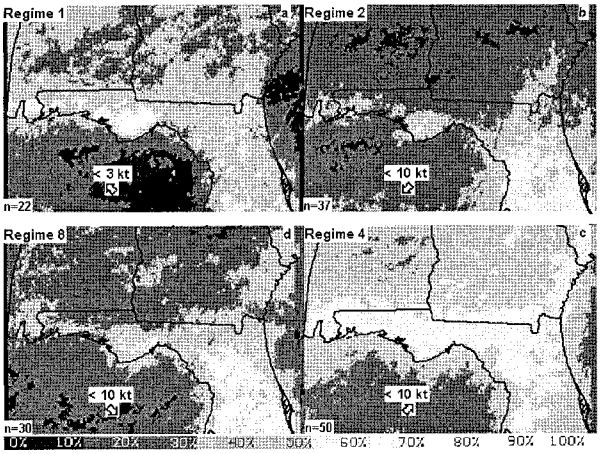

FIG. 8. *GOES-8* 10.7-μm cloud frequency composites by temperature threshold (283 K) for 2115 UTC for (a) regime 1, (b) regime 2, (c) regime 4, and (d) regime 8. The study period includes Jun–Aug for 1996–99. The arrows and wind speeds correspond to the background synoptic conditions for each regime as summarized in Table 1 (n = sample size).

category comprises approximately 25% of regimes 1, 4, and 8 and corresponds primarily to regions over the oceans, bays, and inland rivers. These are regions that tend to have little to no cloud cover in the visible imagery and the same is detected in the 10.7-μm imagery.

Regime 2 has approximately an 8% region of no difference in the cloud frequencies. This regime is characterized by a high pressure system of continental origin in which convection is less active. This type of day will tend to have a large number of small cumulus at this time (1715 UTC) and will tend to show a large discrepancy between the visible and 10.7-μm cloud detection because of the resolution of the imagery.

For the remaining parts of the various image composites, the visible cloud composites predominantly show 6%–35% more cloud frequency than the 10.7-μm composites.

The cloud frequency results based on the 235-K threshold for the 10.7-μm imagery show very little deep convection at this time and are not presented.

b. Afternoon regime composites

Cloud frequency composites are shown in Fig. 6 for regimes 1, 2, 4, and 8 for 2115 UTC, the average time for peak convection for the region. The number of images used to create each composite is displayed in the images. This number may differ from the total number of days designated in Table 2 due to bad or missing satellite images for this particular hour. Under regime 1 (light and variable or light SE flow), there is an area with greater than 70% cloud frequency. This region is located inland and parallel to the coast extending from Tallahassee to the southwest. This point is noteworthy

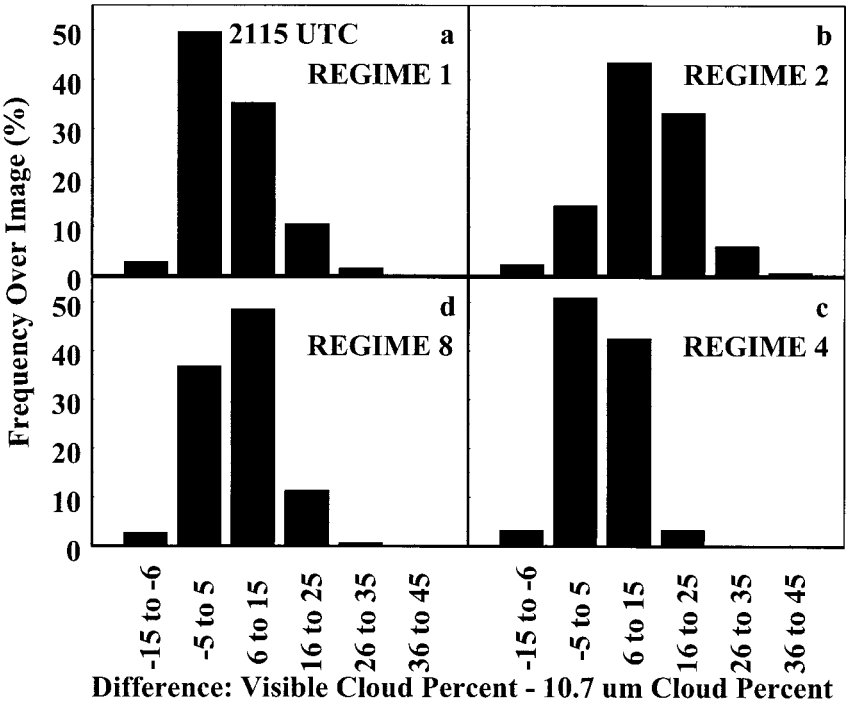

FIG. 9. Histograms of the difference of cloud frequency between the visible composites (Fig. 6) and the 10.7-μm composites (Fig. 8) for 2115 UTC for (a) regime 1, (b) regime 2, (c) regime 4, and (d) regime 8. The x axis represents bins of 10% cloud frequency and the y axis shows the corresponding percentage of occurrence. The -5 to 5 range represents no difference.

for the light and variable or light SE flow typical of regime 1 and for its location on the convex portion of the coastline with Apalachicola at the apex. This higher cloud frequency region is indicative of a merger of the sea-breeze front from the southeast off Apalachee Bay with the sea-breeze front from the southwest coastal regions. All other regimes show few pixels with greater than 70% cloud frequency.

All regimes show the influences of the sea breeze on convection with higher cloud frequency along the coasts and less cloud frequency inland in Georgia and Alabama. Regimes 2 and 8, show significantly less cloud frequency inland than the other regimes. Recall that regime 2 is characterized by a high pressure system to the north of Tallahassee, producing a generally northeasterly flow over the Florida panhandle, while regime 8 usually occurs after passage of a cold front or trough and the winds shift to the north-northwest. Besides less cloud cover inland, both regimes exhibit decreased cloud frequency along the Gulf coast extending from the western side of the Florida panhandle and into southern Alabama.

Regime 4 (W to SW flow) is the most frequently occurring regime (50 images) with nearly two times the number of images as the other regimes. This regime also has the greatest areal coverage of convection at this time of day. Figure 7 quantifies the distribution of cloud frequency ranges over the 2115 UTC image for each of the regimes. Regimes 1 and 4 show that the occurrence of higher cloud frequency has increased over the image, while regimes 2 and 8 show the occurrence of cloud frequency is greater between 20% and 40% and decreases after that.

The cloud frequency results based on the 283-K threshold for 10.7-μm imagery for regimes 1, 2, 4, and 8 at 2115 UTC are presented in Fig. 8. The cloud frequency patterns and cloud frequency amounts correspond well to the visible cloud frequency composites for this time (Fig. 6). The distribution of cloud frequency differences (visible cloud frequency $-$10.7-μm cloud frequency) for each of the regimes is shown in Fig. 9. The -5 to 5 category, which we have designated as no difference, composes a much larger portion of the image at 2115 than at 1715 UTC. Better correlation is also found at 2115 than at 1715 UTC between the visible and 10.7-μm areas (r = 0.85, 0.76, 0.91, and 0.86, respectively, for regimes 1, 2, 4, and 8).

At this time of day, deep convection is being observed and the size of individual cloud elements is larger than 1 km. Because the larger clouds can be detected by both the visible threshold technique and the 10.7-μm threshold technique, the differences between the two techniques are less. This is strongly suggested by regimes 1 and 4. These regimes show 50% of the image as no difference, with the remainder of the image showing a 6%–25% greater cloud frequency from the visible imagery over the 10.7-μm imagery. Regime 2 shows a large percentage of the image (33%) in which the visible

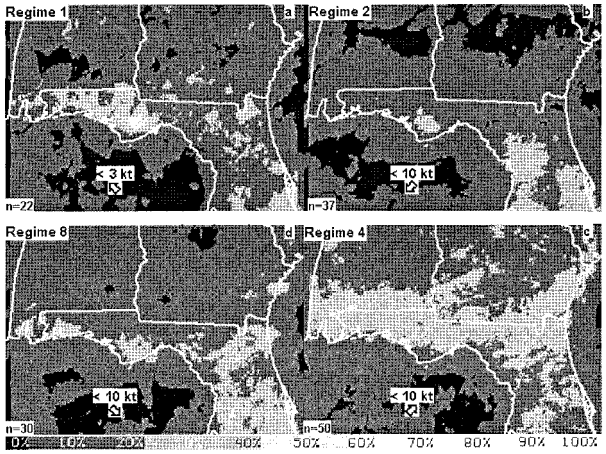

FIG. 10. *GOES-8* 10.7-μm cloud frequency composites by temperature threshold (235 K) for 2115 UTC for (a) regime 1, (b) regime 2, (c) regime 4, and (d) regime 8. The number of images used to create each composite is shown in the lower-left corner of each image. The study period includes Jun–Aug for 1996–99. The arrows and wind speeds correspond to the background synoptic conditions for each regime as summarized in Table 1.

cloud frequency is 16%–25% greater than that determined by the 10.7-μm imagery. This indicates that there are smaller cumulus clouds that are being detected by the visible threshold technique but not the 10.7-μm threshold technique. This again supports one of the characteristics of this regime in that convection is being somewhat suppressed.

The cloud frequency for deep convection for 2115 UTC for regimes 1, 2, 4, and 8 is presented in Fig. 10. These composites were produced with a 235-K temperature threshold of the 10.7-μm imagery. Compared to the visible and 283-K threshold of the 10.7-μm imagery, there is a dramatic decrease in the cloud frequency. Regime 4 has the most widespread deep convection, while regimes 1 and 8 seem to have similar amounts of deep convection, which are distributed differently.

We designate the regions with 40% or more cloud frequency as convective ''hot spots.'' Note in particular for regime 1 the hot spot is located behind the convex portion of the coastline and indicates that the sea-breeze merger is a significant feature under this regime. Other hot spots for this time can be found in the Florida peninsula for regime 8 and in the western portion of the Florida panhandle for regime 4. Although it is not shown here, different hot spots can be found at later times, even after dark, for many of the regimes.

c. Monthly composites

The imagery used for regime composites were readily used to derive diurnal and overall monthly cloud frequency composites. Recall from the previous section and Table 2 that a total of 222 days or 60% of the possible days were designated for the regime study. The

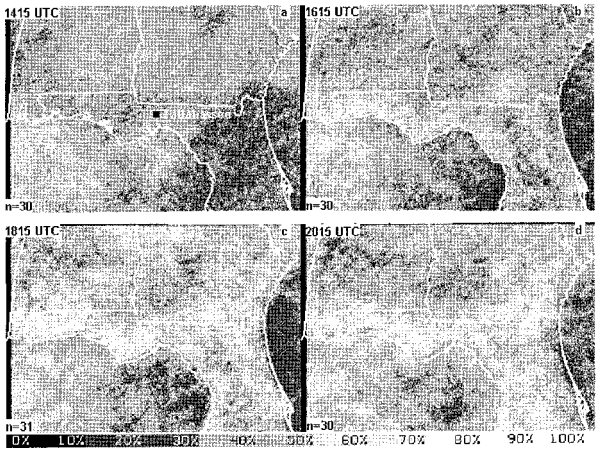

FIG. 11. *GOES-8* visible cloud frequency composites showing the diurnal pattern for the month of Jul 1999 at 1415, 1615, 1815, and 2015 UTC. The number of images used to create each composite is shown in the lower-left corner of each image.

remaining 144 days were characterized by either a disturbed or completely suppressed sea-breeze circulation. The monthly composites provide a different perspective of cloud frequency over northern Florida during the months studied.

Figure 11 shows the diurnal progression of cloud frequency for July 1999. Although these are monthly composites, the daily progression and influence of the sea breeze can be detected. At 1415 UTC (1015 EDT), higher cloud frequencies are seen inland in Georgia and Alabama and are the result of low-level fog and stratus. Other high cloud frequencies are seen offshore in the Gulf of Mexico and represent lingering convection from an overnight land breeze. There is very little cloud cover seen over the Florida peninsula and there are no cloud lines along the coasts that indicate the convergence along the sea-breeze front. By 1615 UTC, cloud frequency has increased along coastal regions and cloud frequency has decreased inland over Georgia and Alabama. For inland areas, this decrease in cloud frequency further confirms that the clouds were low stratus or fog and have dissipated by heating from the sun.

By 1815 UTC there is an increase of cloud frequency along the Gulf and Atlantic coasts, and there is a thin strip along the coasts with lower cloud frequency indicating that the sea-breeze front has progressed inland. At 2015 UTC, the lower cloud frequency regions along the coast are more apparent, particularly on the Atlantic coast, and indicate the inward progression of the sea-breeze front.

Figure 12 shows the overall monthly cloud frequency composites for June, July, and August from 1996–99. The composites are made from the visible imagery and combine the hourly imagery from 1415 to 2115 UTC. Although there is variability from month to month on the location of clouds, the influence of the sea-breeze front on cloud formation can readily be seen in almost all of the composites: there is a higher frequency of clouds along the coastlines and lower cloud frequency inland over Georgia and Alabama. The months of June for 1997–99 do not fit this pattern as well as other months. June of 1997 and 1999 appear to have significant cloud coverage, while June of 1998, with a persistent subsident high, causing record heat across the region, had very little cloud coverage.

During the years of this study (1996–99), there were wide fluctuations in El Niño–Southern Oscillation (ENSO) and these fluctuations were reflected in the Florida weather. In addition to ENSO's possible effect on cloud frequency distributions during these years, nearshore sea surface temperatures (SSTs) and resulting moisture fluxes may also have played a significant role in this pattern. In particular, June of 1998 (very dry) was characterized by unusually cold early season nearshore SSTs, which undoubtedly contributed to the suppressed convection.

4. Summary and conclusions

The concentrations of clouds under the various regimes retain patterns found in Gould and Fuelberg (1996) and Camp et al. (1998). Both the high-resolution (1 km) visible cloud frequency and the coarser-resolution (4 km) 10.7-μm temperature threshold cloud frequency composites assist in quantifying where clouds are more likely to develop throughout the day under the various regimes. Sixty percent of all possible days were assigned to one of nine categories (see Table 1 for regime descriptions). Those days not designated for particular regimes were either completely disturbed synoptically or the sea breeze was suppressed.

Analysis and comments were presented for four wind regimes with contrasting directional wind patterns. Regime 4 (W to SW flow) was the most frequently occurring regime and had the most widespread distribution of cloud frequency, both near the coast and inland. Regime 2, with contrasting E to NE flow, was the next most frequently occurring regime and had lower cloud frequencies than regimes 1 and 4, particularly inland in Alabama and Georgia. Regime 5, with strong W to SW flow (not presented) was the third most frequently occurring regime. Regime 8 with the N to NW flow was the fourth most frequently occurring regime, while regime 1 with light and variable or light SE flow came in fifth.

From previous studies in south Florida and local forecasters experience, we had expected regime 1 (SE flow) to occur more frequently than regime 2 (E to NE flow), but this did not show up in the results. Regime 8 (N to NW flow) also seemed to be occurring more often than expected. It was noted that in addition to the passage of a cold front or trough, a high pressure ridge in the central United States would also cause this regime to occur. We suspect that the years used in the study (1996–99) were unusual in the long-term climatology of the

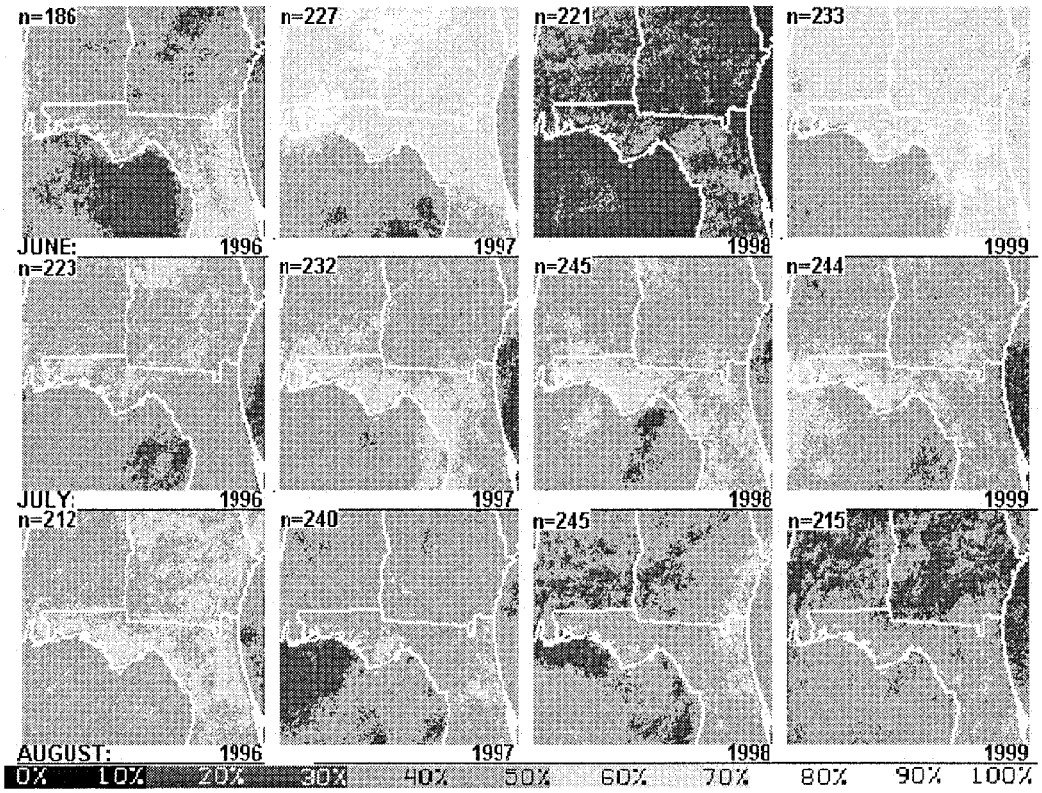

FIG. 12. *GOES-8* monthly visible cloud frequency composites for Jun, Jul, and Aug for each of the years 1996–99. Only images between the hours 1415 and 2115 UTC were used. The number of images used to create each composite is shown in the upper-left corner of each image.

area, but it is also possible that this is a pattern common to north Florida. During these years, there were wide fluctuations in El Niño–Southern Oscillation and these fluctuations were reflected in the Florida weather. In 1996, El Niño was building, 1997 brought the influence of a strong El Niño, and 1998–99 brought the rapid onset and influence of a strong La Niña. As the climatology is expanded into the future and as we compare this dataset with other long-term datasets, such as precipitation and lightning, we hope to be able to address this issue in more depth.

Comparison of the visible cloud frequency composites with those obtained by temperature threshold techniques (283 and 235 K) of the 10.7 μm imagery shed light on the size of the clouds being sampled and the distribution of deep convection. Early in the day, small cumulus on the scale of 1 km were detected by the visible threshold technique, but not by the 10.7-μm 283-K threshold technique. The visible cloud frequency composites showed 6%–35% more cloud cover than that of the 10.7-μm technique. Very little deep convection was recognized by the 235-K 10.7-μm threshold technique at this time.

Early in the day, we also found it both interesting and confirming to be able to detect differences in the location of clear regions over bays and inland rivers under the various regimes with the high-resolution visible composites. This was not as readily discernable using the IR imagery alone.

In the afternoon at 2015 UTC, clouds larger than 4 km were more abundant and the discrepancy between the visible and 10.7-μm cloud frequency composites were less (6%–25%). More deep convection was detected at this time from the 235-K 10.7-μm threshold cloud frequencies than at 1715 UTC with localized regions of higher frequency along the coast. Regions with 40% or greater frequency were designated as convective hot spots.

Monthly composites provided a different perspective on year-to-year and month-to-month variability over the region. These composites included regime days as well as disturbed and suppressed weather days. The influence of the sea-breeze front can readily be seen in the diurnal progression of cloud frequency over a month.

In the future, the visible and infrared cloud frequency composites will be combined with lightning, precipitation, and radar data. With the combined information, we hope to address questions pertaining to frequency and location of rain in association with each of the regimes.

Currently, the regime cloud frequency results are being used extensively in aviation and public forecasting

to supplement existing information. In short-term forecasts, they are being used to ''fine-tune'' convective initiation and the timing of frontal passages. In zone forecasts, cloud frequency information is being used subjectively to produce more accurate and detailed probability of precipitation as well as severe weather or flood potential. In marine forecasts, it has provided more insight into the occurrence of land-breeze convection and the sea fog/stratus potential. In aviation forecasts, the cloud frequency results have also been used subjectively to give better information on ceilings, timing of convection, and convective coverage en route.

Acknowledgments. This work was supported by NOAA Grant NA67RJ0152. The authors would like to thank Irv Watson, Mark DeMaria, and Cindy Combs for their comments on an earlier version of this manuscript.

REFERENCES

Blanchard, D. O., and R. E. López, 1984: Variability of the convective field pattern in south Florida and its relationship to the synoptic flow. NOAA Tech. Memo. ERL ESG-4, Boulder, CO, 77 pp.

——, and ——, 1985: Spatial patterns of convection in south Florida. *Mon. Wea. Rev.,* **113,** 1282–1299.

Camp, J. P., A. I. Watson, and H. E. Fuelberg, 1998: The diurnal distribution of lightning over north Florida and its relation to the prevailing low-level flow. *Wea. Forecasting,* **13,** 729–739.

Garreaud, R. D., and J. M. Wallace, 1997: The diurnal march of convective cloudiness over the Americas. *Mon. Wea. Rev.,* **125,** 3157–3171.

Gibson, H. M., and T. H. Vonder Haar, 1990: Cloud and convection frequency over the southeast United States as related to small-scale geographic features. *Mon. Wea. Rev.,* **118,** 2215–2227.

Gould, K. J., and H. E. Fuelberg, 1996: The use of GOES-8 imagery and RAMSDIS to develop a sea breeze climatology over the Florida panhandle. Preprints, *Eighth Conf. on Satellite Meteorology and Oceanography*, Atlanta, GA, Amer. Meteor. Soc., 100–104.

Kidder, S. Q., and T. H. Vonder Haar, 1995: Radiative transfer. *Satellite Meteorology: An Introduction.* Academic Press, 47–85.

Klitch, M. A., J. F. Weaver, and F. P. Kelly, 1985: Convective cloud climatologies constructed from satellite imagery. *Mon. Wea. Rev.,* **113,** 326–337.

Knapp, K. R., and T. H. Vonder Haar, 2000. Calibration of the *Eighth Geostationary Observational Environmental Satellite* (*GOES-8*) image visible sensor. *J. Atmos. Oceanic Technol.,* **17,** 1639–1644.

Lazzara, M. A., and Coauthors, 1999: The Man computer Interactive Data Access System: 25 years of interactive processing. *Bull. Amer. Meteor. Soc.,* **80,** 271–284.

Menzel, W. P., and J. F. Purdom, 1994: Introducing GOES-I: The first of a new generation of Geostationary Operational Environmental Satellites. *Bull. Amer. Meteor. Soc.,* **75,** 757–781.

Molenar, D. A., K. J. Schrab, and J. F. W. Purdom, 2000: RAMSDIS contributions to NOAA satellite data utilization. *Bull. Amer. Meteor. Soc.,* **81,** 1019–1030.

Rabin, R. M., and D. W. Martin, 1996: Satellite observations of shallow cumulus coverage over the central United States: An exploration of land use impact on cloud cover. *J. Geophys. Res.,* **101** (D3), 7149–7155.

Reinke, D. L., C. L. Combs, S. Q. Kidder, and T. H. Vonder Haar, 1992: Satellite cloud composite climatologies: A new high-resolution tool in atmospheric research and forecasting. *Bull. Amer. Meteor. Soc.,* **73,** 278–286.

Schiffer, R. A., and W. B. Rossow, 1983: The International Satellite Cloud Climatology Project (ISCCP): The first project of the World Climate Research Program. *Bull. Amer. Meteor. Soc.,* **64,** 779–784.